

The millimeter- and submillimeter-wave spectrum of the *trans-gauche* conformer of diethyl ether

Ivan Medvedev^a, Manfred Winnewisser^{a,*}, Frank C. De Lucia^a, Eric Herbst^a, Ewa Białkowska-Jaworska^b, Lech Pszczółkowski^b, Zbigniew Kisiel^b

^a Department of Physics, The Ohio State University, Columbus, OH 43210-1106, USA

^b Institute of Physics, Polish Academy of Science, Al.Lotników 32/46, 02-668 Warsaw, Poland

Received 23 March 2004; in revised form 8 June 2004

Available online 22 July 2004

Dedicated to Dr. Jon T. Hougen in appreciation of his contributions to the field of theoretical molecular spectroscopy

Abstract

The results of a first investigation of the rotational spectrum of the *trans-gauche* conformer of diethyl ether are reported. Two spectrometers have been used to measure the spectrum in the millimeter-wave and submillimeter-wave regions and a total of 1090 absorption line frequencies in the range 108–366 GHz were obtained and analyzed. Of these lines, 902 were measured with a spectrometer employing the fast scan submillimeter spectroscopic technique (FASSST) at Ohio State and the remaining 188 were measured with the phase-lock two-loop system (PLL) in Warsaw. The spectrum was fit to within experimental accuracy with the use of the *A*-reduced Watson Hamiltonian. Based on relative intensity measurements, the percentage of diethyl ether at room temperature in the *trans-gauche* conformer was found to be 30.5(13)%, in good agreement with prior spectroscopic values and an *ab initio* determination based on an energy difference of 5.40 kJ mol⁻¹ (452 cm⁻¹) between the excited *trans-gauche* and ground *trans-trans* conformers. This work also stimulated a critical evaluation of the data acquisition and calibration procedure of the FAAAST spectrometer, the results of which will be discussed.

© 2004 Elsevier Inc. All rights reserved.

Keywords: *trans-gauche* conformer of diethyl ether; FASSST; PLL; Astrophysics; Molecular spectroscopy

1. Introduction

For many years, it has been our exceedingly good fortune to interact with Jon Hougen on a variety of matters spectroscopic. Although the subject of our present spectroscopic study—the *trans-gauche* (*tg*) isomer of diethyl ether—is too stable and regular to have excited Jon's deep interest, it is a conformer of the ground *trans-trans* (*tt*) species, and so possesses some similarity to Jon's beloved excited torsional states. Our interest in the *trans-gauche* conformer followed our earlier study of the millimeter-wave and submillimeter-wave spectrum of

the *trans-trans* conformer [1]. In that study, we used four different spectrometers to assign and analyze many lines at frequencies through 350 GHz. The work was undertaken to determine the frequencies of lines that might put the tentative detection of diethyl ether in the interstellar medium [2] on a firmer basis. This tentative detection was claimed in the direction of three warm regions of dense interstellar clouds surrounding newly-born high-mass stars. Known as hot molecular cores, these regions possess densities (10⁶–10⁷ cm⁻³) and rotational temperatures (100–300 K) in excess of standard values in the clouds [3]. Unlike the unsaturated chemistry dominant in colder sources, a saturated chemistry dominates in hot cores, with simple organic molecules thought to arise from a complex synthesis involving chemistry on

* Corresponding author. Fax: 1-614-292-7557.

E-mail address: winnem@mps.ohio-state.edu (M. Winnewisser).

the surfaces of tiny dust particles followed by evaporation. Moreover, the temperatures are warm enough and the radiation field strong enough near to the star that molecules in excited torsional and even vibrational states have been detected.

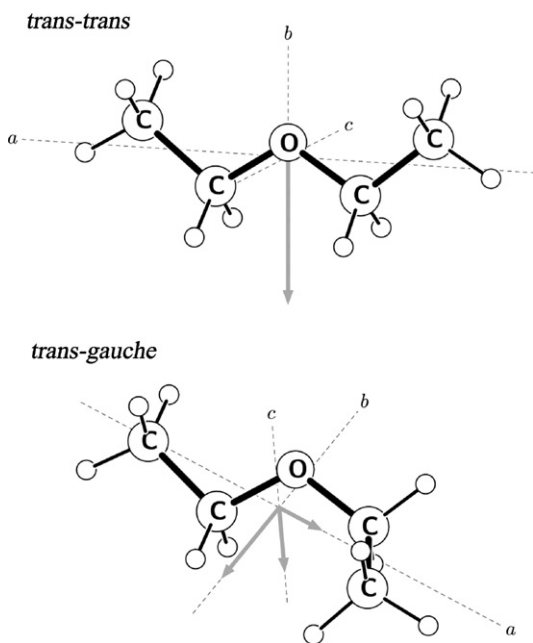


Fig. 1. Comparison of the geometries of the *trans-trans* and the *trans-gauche* conformers of diethyl ether. Both structures are given in the principal axis systems of inertia together with the orientation of the respective components of the permanent electric dipole moments.

After the assignment in the laboratory of over 1000 lines arising from rotational transitions in the ground vibrational state of the *trans-trans* conformer, it became clear that at least one more conformer of diethyl ether must exist together with rotational transitions arising from molecules in excited vibrational states of perhaps both conformers. Ab initio predictions concerning the minimum energy of the low-lying *trans-gauche* conformer [1] and references therein show this conformer to be the most likely source of a large proportion of the hitherto unassigned spectral lines. Calculated structures of the *trans-gauche* and *trans-trans* conformers are depicted in Fig. 1.

A detailed analysis based on data from two spectrometers and discussed in this paper has yielded over 1000 lines belonging to the ground vibrational state of the *trans-gauche* conformer. To the best of our knowledge, the rotational spectrum of this conformer had not been studied previously. The co-existence of spectral lines from both conformers is clearly illustrated in Fig. 2, which shows a part of the millimeter-wave spectrum we have measured around 208 GHz. The rotational spectrum of the *trans-gauche* form of diethyl ether differs in significant detail from that of its *trans-trans* counterpart, a fact that has made the analysis of the many spectral lines recorded easier than it might have been. Unlike the *trans-trans* form, which possesses a dipole component along only one axis, the *trans-gauche* conformer has three non-zero components. Moreover, rotational constants of the two conformers are suffi-

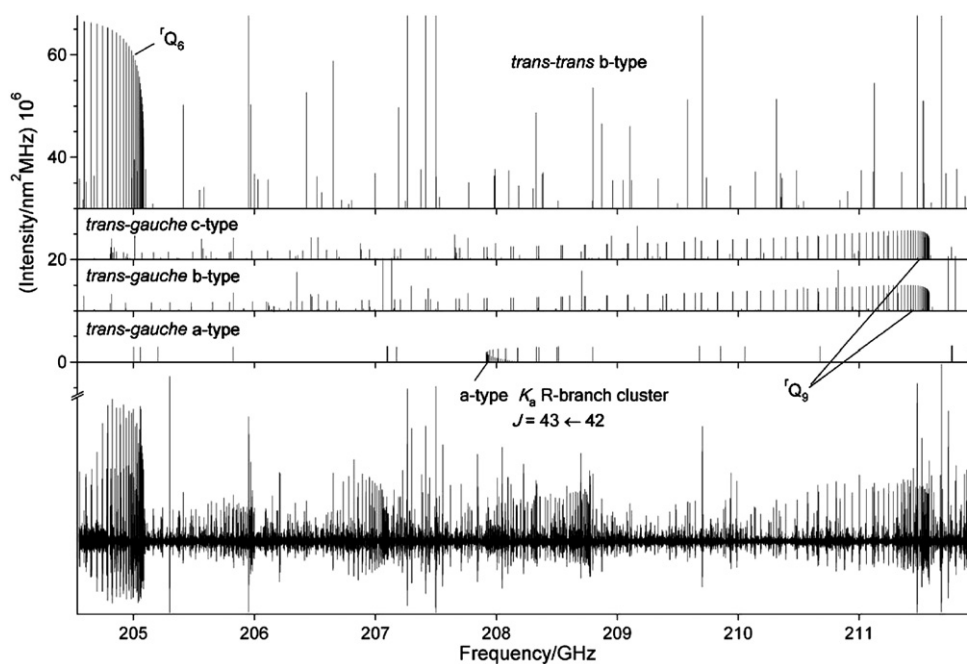


Fig. 2. Part of the millimeter-wave spectrum of diethyl ether. The top four traces show the theoretical frequency and intensity predictions for both *trans-trans* and *trans-gauche* conformer transitions, using the spectroscopic constants in Table 1 and the respective dipole moment components discussed in the text. The bottom trace represents the experimental spectrum.

ciently different so that strong overlapping of lines is often avoided.

Prior to our experimental work, the *trans-gauche* conformer had been studied by electron diffraction [4] and Raman spectroscopy in the gas phase, and by liquid-phase vibrational spectra [5,6]. All of those studies indicate that at room temperature the percentage of ether in this conformer is approximately 25–35%, and that it lies approximately $5\text{--}6\text{kJmol}^{-1}$ or $418\text{--}502\text{cm}^{-1}$ above the ground state conformer, in agreement with ab initio determinations [4]. In astronomical units, the conformer lies approximately 600–700 K above the ground conformer, making its detection in hot molecular cores a distinct possibility if the tentative detection of the *trans-trans* form is correct.

The remainder of the paper is divided as follows. In Section 2, we discuss the two spectrometers used to obtain the spectrum of the *trans-gauche* conformer in the frequency range 108–366 GHz in more detail than is customary to bring out new developments and improvements as well as the calibration procedures. In Section 3, the measured rotational spectrum is discussed and the details of our analysis mentioned. Experimental and theoretical determinations of the population of the *trans-gauche* conformer at room temperature are presented in Section 4, while the paper concludes with a discussion in Section 5.

2. Experimental details

Two different spectrometers were used in this work. The spectrometers were of considerably different design but utilized the same radiation sources.

2.1. The Columbus FASSST spectrometer

Since the early reports on the FASSST approach [7–9], some time has elapsed and substantial advances in the FASSST spectrometer system have been made in the realm of spectrometer and computer hardware and the spectroscopic software to facilitate the assignment of complex molecular spectra.

The FASSST technology makes use of backward-wave oscillators (BWOs) as radiation sources for the millimeter- and submillimeter-wave region. The intrinsic property of a BWO is that its output frequency can be tuned via the electron acceleration voltage over a wide range (10–100 GHz in a very short time of $\sim 1\text{s}$) with a remarkably high spectral purity, thus freezing out most frequency instabilities. The BWOs used in our experiment were produced by ISTOK Research and Development Company of Fryazino, Moscow Region, Russia.

A block diagram of the current FASSST spectrometer is shown in Fig. 3. The essential elements are: (a) a radiation source (BWO) placed in the field of a strong

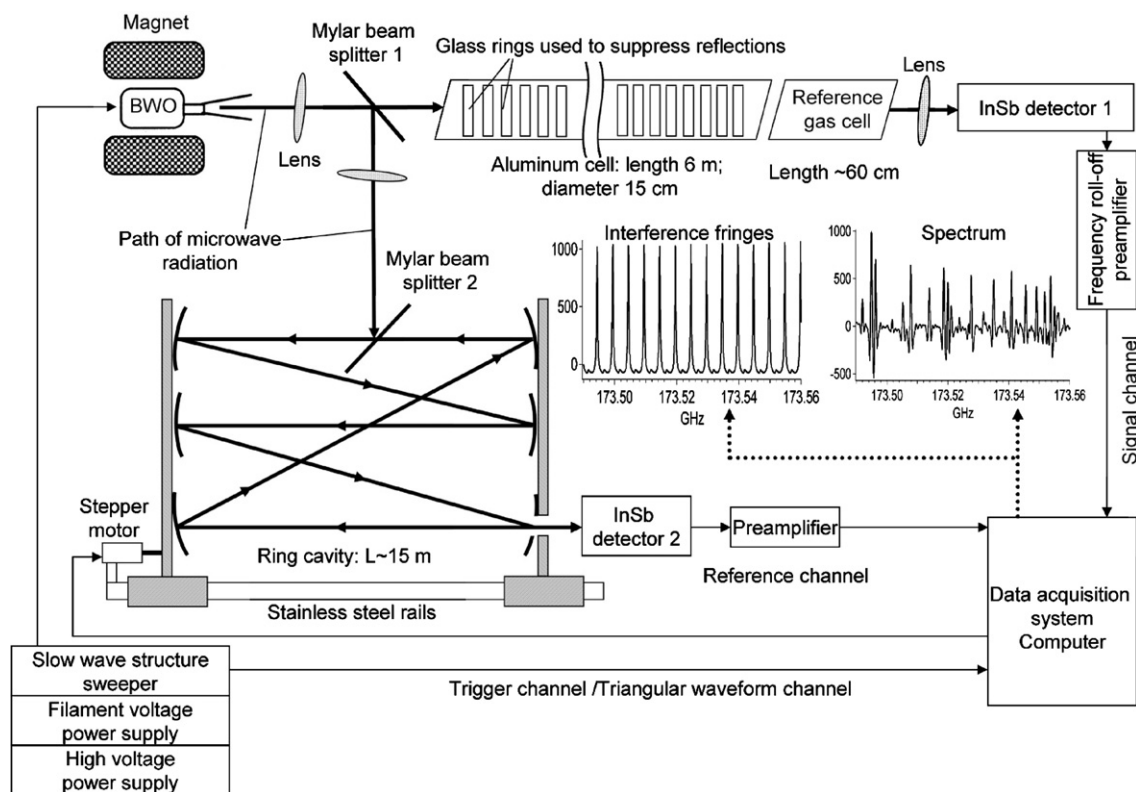


Fig. 3. Block diagram of the Columbus FASSST spectrometer. The interference fringes are produced in the present set-up by a ring cavity arrangement.

permanent magnet or electromagnet; (b) power supplies for BWO and magnet; (c) an aluminum absorption cell 6 m in length and 15 cm in diameter; (d) a reference-gas cell with a length of 60 cm; (e) two beam splitters and a cavity that produces the interference fringes used as frequency markers in the calibration procedure; (f) two InSb hot-electron detectors, one for the signal channel and one for the reference channel; (g) a sweeper unit, which produces the electron acceleration voltage applied to the BWO slow-wave structure; (h) an amplifier with adjustable frequency roll-off; and (i) a data acquisition system with computer. We will discuss the characteristics and properties of some of these spectrometer constituents.

2.1.1. Backward wave oscillators

A set of three BWOs operating in the frequency ranges from 108 to 190, 189 to 252, 260 to 295 and 297 to 366 GHz was used to acquire the diethyl ether spectrum. BWO tubes operating in the frequency range below 190 GHz are air cooled and come pre-assembled with a permanent magnet. The higher frequency tubes are mounted in an electromagnet adjustable from 0.5 to 1.1 T, depending on the requirements of each tube. The output waveguide has a horn antenna attached to it for collimation of the radiation. A set of lenses made of Teflon and/or polyethylene is used to improve the collimation of the microwave beam.

The choice of the operating parameters of the FASSST spectrometer, such as sweep rate and the bandwidth of the signal processing channel, is determined by the physical properties and in particular the response times of the system components. The main sources of noise or error are fluctuations in the BWO output frequency that are caused in part by the 60 Hz modulation introduced by the AC filament current, and in part by mechanical vibrations of the cavity or by any perturbation with a time constant smaller than the time of the sweep across a single spectral feature.

The frequency source is operated in a free-running mode. By applying a triangular wave form to the BWO, the output frequency can be swept rapidly. The short term frequency stability is ~ 10 kHz. Thus, spectral absorption features with a width of 500 kHz (Doppler width) are not significantly broadened. The intrinsic spectral purity of BWOs and their high voltage sensitivity require an electronic filtering of the electron acceleration voltage to obtain a residual noise of less than 2 mV. This filtering is carried out in the sweep generator. A sweep rate of 10–20 GHz/s applied to a particular BWO freezes these inherent low frequency fluctuations in the BWO's output frequency on the time scale of the sweep across a single absorption line. Furthermore, a high sweep rate results in a signal recovery frequency that largely eliminates $1/f$ noise and the need for a superposed high modulation frequency.

2.1.2. Calibration, Fabry–Perot cavity and absorption cell

To achieve an accurate frequency calibration of the individual absorption lines in the FASSST spectra, we use the well-predicted line positions of a reference gas, which is usually sulfur dioxide, and is contained in the second absorption cell as shown in Fig. 3. The known frequencies of the reference gas lines used in the calibration procedure enable us to determine the reference cavity mode spacing and absolute frequency. The frequency of each individual interference fringe is calculated from a count of cavity modes, and an interpolation between the positions of adjacent fringes relative to the position of an unknown absorption line yields the calculated line position.

To enhance the experimental flexibility, a compact Fabry–Perot cavity was designed and assembled (see Fig. 3). The new cavity design consists of two vertical aluminum mirror support plates spaced approximately 3 m apart. Each mirror support carries six copper mirrors and is mounted on a movable platform which can slide along two solid stainless steel rails. The diameter of each copper mirror is 15 cm and its radius of curvature 3 m. This arrangement of the new mirror system provides flexibility in the cavity configuration. The initial configuration of 11 traversals resulted in a cavity length of 33 m and a spacing of ~ 5 MHz between adjacent interference fringes. The problem with this setup was, however, that part of the radiation inside the cavity could couple back into the spectrometer system at the beam splitter, thus traveling all the way back to the radiation source, reflecting, and entering the spectral channel. The problem of the power reflections was resolved by averaging consecutive scans and incrementally changing the total length of the cavity between sweeps. A stepper motor was attached to one of the aluminum mirror support plates to change the spacing between the plates by ~ 1 μm , which changes the frequency positions of the fringes by ~ 100 kHz at 300 GHz. The co-addition of scans significantly reduces the fringe feedthrough. To further reduce the feedthrough of the cavity fringes into the signal channel, the alignment mode of the mirrors was changed to form a ring cavity. In this configuration the cavity marker spacing increased to ~ 9.5 MHz. No significant change in the calibration accuracy was observed. The *trans-gauche* diethyl ether data reported here were taken with the cavity aligned as a Fabry–Perot system.

To enable heating and cooling of the gas cell, the glass absorption cell was replaced with a 6 m long, 15 cm diameter aluminum pipe with Teflon windows. The insertion of glass rings into the aluminum cell substantially reduces reflections on the cell wall and thus smoothes the baseline signal.

2.1.3. Detectors and preamplifiers

Two hot electron InSb bolometers cooled to liquid ^4He temperature were used as detectors. With a band-

width of 1 MHz such a detector is capable of reproducing $\sim 5 \times 10^5$ Doppler limited spectral features per second. The Doppler line width is ~ 500 kHz at 300 GHz for diethyl ether. This translates into 250 GHz/s maximum scan rate based on the detector specifications. However, the typical scan rate is 10–20 GHz/s. This results in the signal peaking at ~ 20 kHz.

Each InSb bolometer is connected to a QMC low noise preamplifier. For the spectrum channel this preamplifier is followed by a SRS SR560 amplifier with adjustable bandpass. The low frequency roll-off is typically set to decrease the baseline variations and eliminate most of the $1/f$ noise. This selection transforms the Doppler line shape function of the absorption signal into an approximate first derivative. The high frequency roll-off, typically set at 30 kHz, decreases the high frequency noise. For the reference channel the QMC preamplifier is followed by a SRS SR560 amplifier with a bandpass of DC to 1 MHz.

2.1.4. Data acquisition system

A dual processor workstation (Athlon 1.8 GHz, 2 Gbytes RAM) is currently used to control the experiment. The dual CPU configuration allows us to acquire and process large quantities of data simultaneously. For example, 400 scans over a 60 GHz spectral interval at a resolution of 10 data points/MHz produces ~ 2 Gbytes of data files. We employ a DVD writer to routinely backup the recorded spectra. A digitizer (NI PCI-6110) provides, in addition, independent variable gain control for all four channels. The digital output of the board is used to control the stepping motor for changing the length of the Fabry–Perot cavity between scans.

The data acquisition is triggered by a signal from the high voltage BWO sweeper unit. The data acquisition system digitizes the input from four channels: (1) signal (spectrum) voltage, (2) reference voltage (cavity fringes), (3) voltage ramp signal, and (4) voltage trigger signal. The spectrometer data acquisition software is written in Labview [10] and has several operational modes. For example, if the software is operating in the averaging mode it is capable of enabling the stepper motor to change the cavity length. All acquired data for each individual scan or sweep are saved as individual files for later processing by the calibration software. The frequency–voltage function depends critically on the thermal environment of the BWO. Thus, it was found mandatory to calibrate each sweep separately before the individual sweeps could be co-added.

The calibration software, an earlier version of which was discussed in [7], is based on the IgorPro package [11], which provides a convenient graphical and programming interface. It also allows us direct access to the computer memory, which significantly increases the processing speed. In the averaging mode, the software automatically calibrates and linearizes in frequency each individual scan and co-adds all calibrated scans.

The following steps are undertaken to calibrate individual data files. Trigger channel information is used to identify the margins of the sweep. The initial estimate of the frequency range is obtained from the data in the voltage ramp channel and the stored BWO frequency–voltage characteristics. The spectral channel is then convolved with a first derivative Gaussian line shape to reduce the baseline signal and to transform the signal of the spectral line shape function into an approximate second derivative line profile. The calibration lines, taken from the JPL catalog [12] as reference, are identified in the spectrum by a cross-correlation technique. This information is then used together with the fringe peak positions in a least-squares fit to calculate the frequencies of the cavity modes. In the last step, the calibration software calculates the frequency position for each data point in the spectrum data array. Finally, a linearized spectrum is calculated via interpolation.

The data averaging mode has become the standard for recording spectra with the FASSST spectrometer. The feedthrough of the interference fringe signal into the spectrum channel is greatly and effectively reduced by averaging scans with different settings of the cavity length. The present spectral data of the *trans–gauche* diethyl ether spectrum were recorded with the co-addition of 400 scans. The double benefit is an improved signal-to-noise ratio of the final spectrum and reduced fringe feedthrough in comparison with one single scan recorded with the earlier version of the FASSST system. The final composite FASSST spectrum of diethyl ether ranges from 108 to 366 GHz with small frequency gaps from 252 to 260 GHz and from 295 to 297 GHz. It should be noted that only scans upwards in frequency were recorded and are used in this work.

2.2. The Warsaw PLL spectrometer

As in the preceding investigation of the *trans–trans* conformer [1], rotational spectra were also recorded on the millimeter-wave spectrometer in Warsaw, which has been described in [13–15]. This spectrometer contains the same mm-wave BWO sources from the ISTOK Research and Development Company mentioned above and provides a natural reference point for the FASSST design. It is therefore useful to briefly discuss its construction, shown schematically in Fig. 4. The Warsaw spectrometer records spectra using traditional source modulation and synthesized, slow frequency sweeps, while the overriding design criterion has been to reach satisfactory performance at the lowest budget. Frequency stabilization is achieved by means of two phase lock loops (PLLs) and is based on the HP-8648C economy RF signal generator, which is in fact a low switching noise synthesizer operating up to 3.2 GHz. In the first stabilization loop, PLL₁, the synthesizer signal is used to stabilize the output from a solid state HP-8620B/

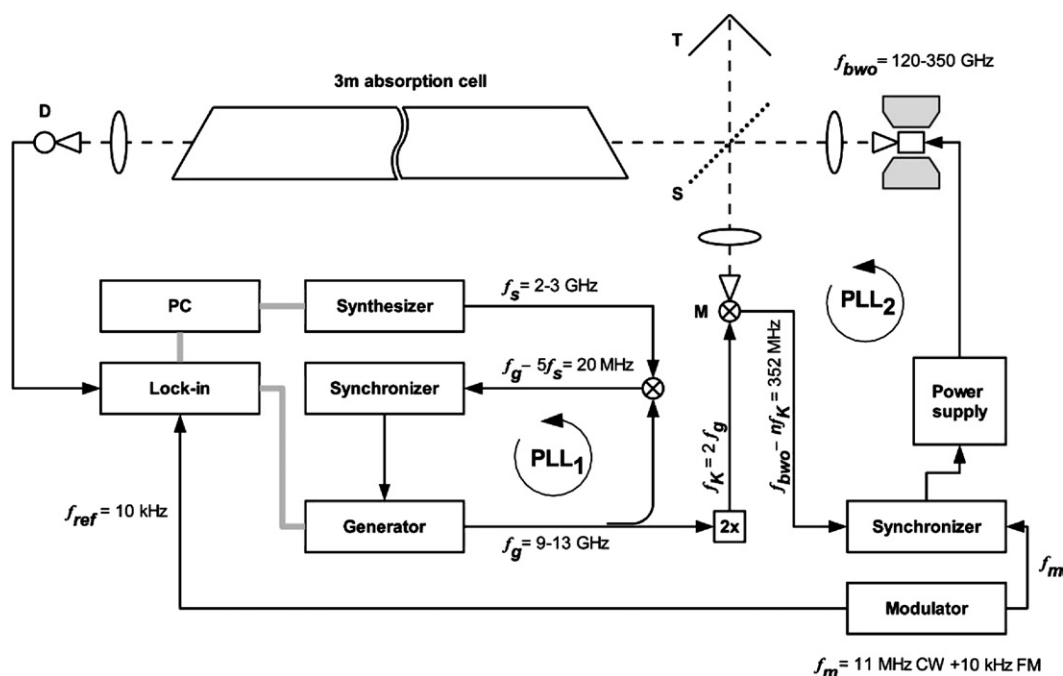


Fig. 4. Schematic diagram of the Warsaw millimeter-wave spectrometer, which uses the same BWO sources as the FASSST system. This spectrometer was designed along the more traditional principle of phase lock loop (PLL) frequency stabilization and source modulation, and was optimized for economy of construction.

86290B microwave generator by utilizing the popular HP8709A synchronizer, which maintains a constant intermediate frequency (IF) of 20 MHz. Output of the stabilized generator is multiplied with an active doubler to constitute the local oscillator signal for the second stabilization loop, PLL₂. The second loop is closed by a synchronizer made in the Lille laboratory, which operates at an intermediate frequency (IF) of 352 MHz. Source modulation is applied in the second loop by superimposing a small FM modulation onto the 11 MHz external IF reference input to the synchronizer, which is then internally multiplied by a factor of 32. This reference signal is conveniently generated in another budget device, an HP-33120A function generator employing direct digital synthesis. The performance of both stabilization loops is continuously monitored, the frequency f_K is checked with a frequency counter, and the BWO correction signal is displayed on an oscilloscope to check the quality of the applied modulation. Each spectrum is recorded as an average of up and down scans. Lock-in detection with the second harmonic of the modulation frequency leads to a second derivative of the line-profile function.

Both the millimeter-wave detector *D* and the high-frequency harmonic mixer *M* are room-temperature devices using Farran honeycomb GaAs Schottky diode chips, which are placed in the classical King and Gordy-type contact-diode mounts [16]. The beam-splitter *S* is a wire grid polarizer made of parallel 10 μm tungsten wires at 50 μm spacing. A rooftop tuner *T* is used to ensure

optimum alignment of the two arms of the spectrometer. Various steps have been taken to combat standing waves. The windows of the absorption cell are inclined, there are many non-reflecting diaphragms in the optical tract, and additional filtering wire grids are inserted into the cell arm when necessary. Furthermore, an efficient baseline subtraction algorithm is implemented in the spectral viewing program SVIEW [17], which determines the baseline by means of least squares smoothing. The use of BWO sources endows this spectrometer with broad-band scanning capabilities. For various practical reasons, individual scans are normally limited to 0.5 GHz. Spectra of diethyl ether were recorded on a sample at a pressure of ~ 20 mTorr held in a 3 m long brass absorption cell of 10 cm internal diameter. In view of the availability of the FASSST spectrum, PLL spectra were only recorded with the OB-30 source in the spectral region from 252 to 342 GHz.

2.3. Comparison of PLL and FASSST spectra

Acquisition of extensive rotational spectra of diethyl ether with two different spectrometers employing the same radiation sources allows various high precision instrumental comparisons to be made. In particular, it is possible to benchmark the performance of the FASSST spectrometer.

Some useful information can be gleaned from Fig. 5, which presents a direct comparison of the same relatively dense spectral segment recorded with the two spectrometers.

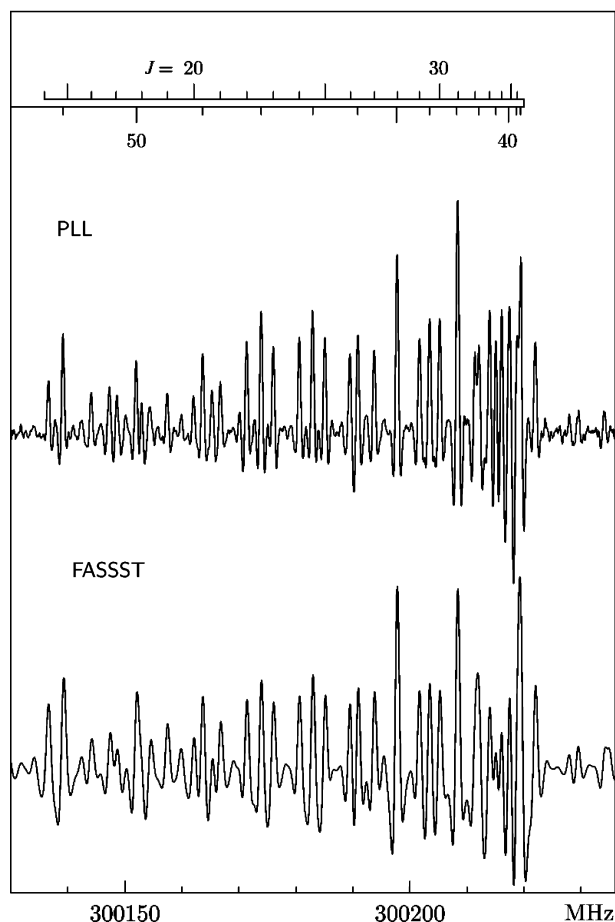


Fig. 5. Comparison between FASSST and traditional PLL millimeter-wave spectra of *trans-gauche* diethyl ether, covering the expanded bandhead of the $K_a=14\leftarrow 13$ Q -branch. The PLL recording has a somewhat higher resolution, although the FASSST lineshape is, on average, found to be only about 50% broader.

ters. It is apparent that the PLL spectrometer has somewhat higher resolution which is, in principle, only limited by the Doppler profile of the absorption lines. The spectral purity of the locked radiation signal is considerably narrower than the molecular linewidth, and careful control of experimental conditions allows even Lamb-dip sub-Doppler features to be observed. The FASSST lineshape is visibly broader, primarily due to the filtering and signal convolution made in the detection channel. In spite of these additional factors, it is found that the FASSST lineshape is, on average, only about 50% broader than the PLL one. In the densest part of the spectrum in Fig. 5 the broader FASSST lineshape results in more pronounced blending, while in the case of more isolated lines it should not be an impediment to precise frequency measurement, especially since the FASSST spectrum is recorded at a very good signal-to-noise level.

The second issue is the accuracy of transition frequencies derived from the FASSST spectrum. This is addressed in Fig. 6, where external calibration of the FASSST frequencies has been made in two different ways. Fig. 6A is a plot of simple frequency differences between frequency measurements of the same lines in FASSST and PLL spectra. This plot results from correlation of raw peakfinder outputs and rejection of evident mismatches. Some of the apparent noise and the remaining outliers are attributable to differences in blending of lines in spectra from the two spectrometers. Nevertheless a general clear trend of systematic frequency deviations is visible. In order to confirm that there is no effect coming from the PLL frequencies, a second calibration is shown in Fig. 6B. This calibration is based on the assumption that frequencies of identified lines in the range of Fig. 6 are expected to be calculable to better or much

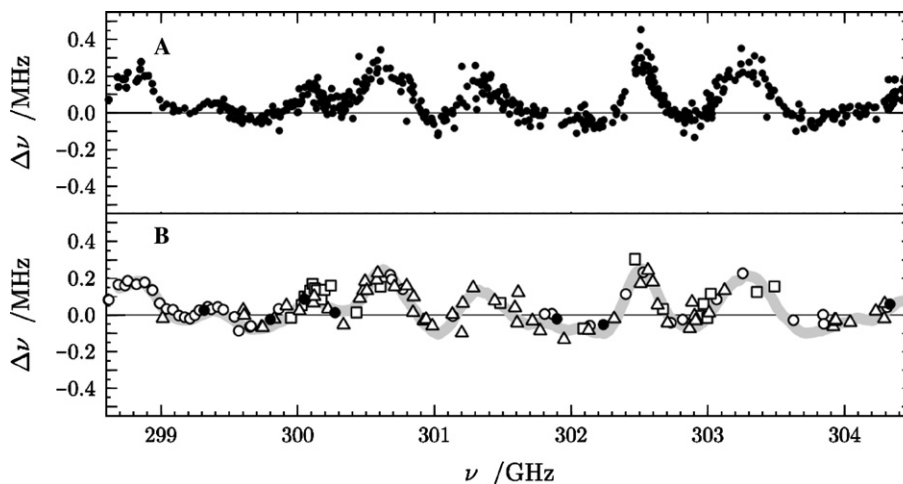


Fig. 6. The accuracy of calibration of the FASSST spectrum as determined from: (A) comparison of measured line frequencies from FASSST and PLL spectra of diethyl ether and (B) comparison of FASSST frequencies with frequencies calculated from the best spectroscopic constants for the ground (open circles) and excited vibrational states (triangles) of *trans-trans* diethyl ether, the ground state of *trans-gauche* diethyl ether (squares), and SO_2 (full circles). The shaded line in (B) denotes the average of the dependence obtained in (A).

better than 0.10 MHz, since precise spectroscopic constants have already been determined for several of the involved spectroscopic species. Thus a difference plot between the FASSST and the predicted frequencies would be expected to parallel the plot in Fig. 6A, as is indeed found to be the case. The plots in Fig. 6 can therefore be regarded as an absolute frequency calibration of the FASSST spectrum of diethyl ether over a frequency span of almost 6 GHz, and allow for much useful insight. The root mean square deviation in Fig. 6A, with inclusion of the outliers, is calculated to be 0.125 MHz, about twice that found for the entire data set, substantiating the assumption of 0.10 MHz normally made for the accuracy of FASSST line frequencies. Interestingly the plots in Fig. 6 are not centered on zero but have an average positive deviation of 0.06 MHz. The error waveform is also seen to be a rather long range one, with a period in the region of 0.5 GHz and, in the worst but relatively rare cases, the deviation from the true frequency may exceed 0.3 MHz. On the other hand, while locally the frequency deviations have a systematic nature, these are expected to become statistical for the large data sets normally extracted from FASSST spectra. In summary, although there are still some performance penalties associated with the current implementation of the FASSST technique, in determining spectral parameters these have been more than compensated by rapid access to an almost uninterrupted 250 GHz segment of the rotational spectrum of diethyl ether. It is also clear that a factor of two improvement in the FASSST

calibration procedure would take the frequency accuracy of the FASSST spectra to a level hitherto thought to be possible only with PLL techniques.

The systematic trends shown in Fig. 6 suggest that it is possible to improve the accuracy of the frequency measurement of the FASSST system. As a first step, we employed a statistical analysis and individually calculated the error distributions and the rms deviations of the PLL data and the FASSST data in the fit of the *trans-gauche* diethyl ether. We found for both data sets close to Gaussian error distributions and 0.052 and 0.079 MHz rms deviations, respectively, roughly consistent with our 2:1 accuracy estimate used in the weighting of the data. This indicates that the spectral region displayed in Fig. 6 probably exhibits the largest deviations in the measurements of the present FASSST data set. It is thus the optimum region for tests of the efficacy of measures to eliminate the type of errors discussed above.

The frequency dependence of the systematic trends displayed in Figs. 7c–e is similar to the reproducible small-scale [7] variation in the frequency–voltage characteristics of the BWO which are reproduced in Figs. 7a and b. It suggests that the sweep rate variation needs to be considered more carefully. Because of time delays and phase shifts in the signal processing, the peak positions of the experimental lineshapes, that approximate second derivatives, are shifted in time. *If* all lines, including the calibration lines, have the same line width, *and if* the sweep rate is constant during the sweep, the delay occurring in both the calibration lines and the spectro-

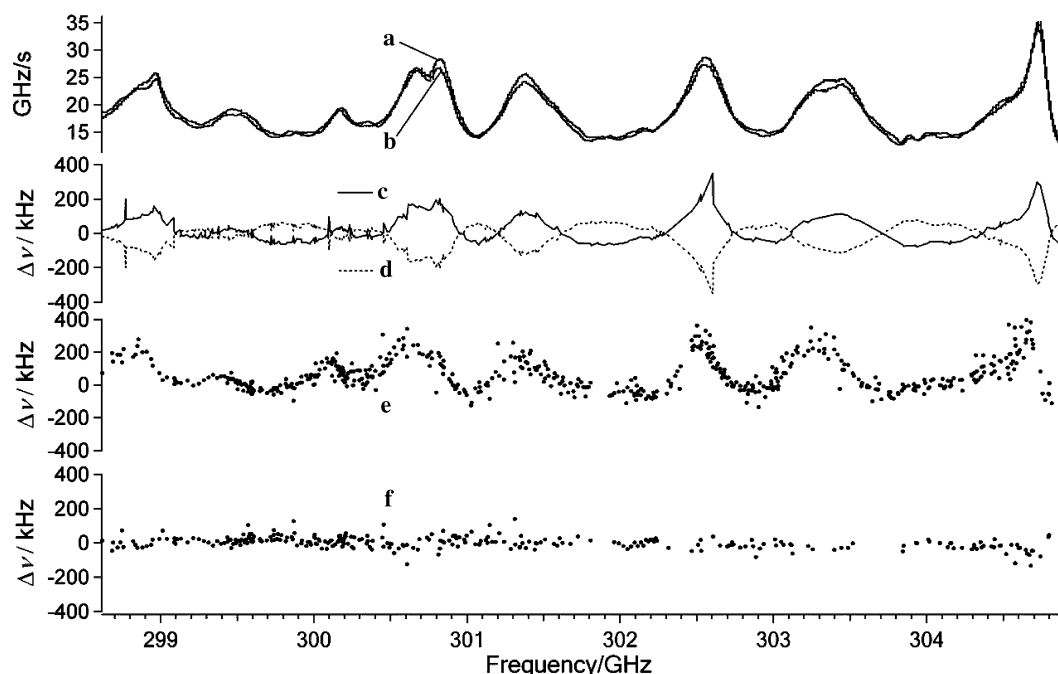


Fig. 7. Small-scale structure of the sweep rate for sweeps upwards and downwards in frequency, as displayed in traces (a) and (b), respectively. Average of up-down sweep peak positions minus down sweep peak positions (c). Average of up-down sweep peak positions minus up sweep peak positions (d). FASSST peak positions using sweep up in frequency only minus PLL peak frequencies (e). PLL peak positions minus FASSST peak positions using average of up-down sweeps (f).

scopic lines to be measured cancel. To test this hypothesis, we determined the actual sweep rates in up and down frequency sweeps, shown in Figs. 7a and b. There exists an expected similarity between the up and down sweep rates as a function of frequency. The small difference between the sweep rate excursions in Figs. 7a and b can be explained by the difference in the thermal history of the BWO in the up and down sweep modes. Our test (diethyl ether) data set consisted of the co-addition of 100 scans up in frequency and 100 scans down in frequency. With the traditional solution of averaging the peak frequencies obtained from the up and down sweeps, we obtained the deviations that are plotted in Figs. 7c and d. When this is done, Fig. 7f results, showing that the systematic shifts displayed in Figs. 6 and 7e have been eliminated (rms deviation ~ 34 kHz) when the up and down averaged line positions of the FAAAST data are subtracted from the PLL data.

3. Rotational spectrum and analysis

Results from previous gas-phase electron diffraction work [4] and vibrational spectroscopy of diethyl ether [5,6] suggest that the room temperature population of the *trans-gauche* conformer is near 30%. Supporting ab initio calculations were carried out at the MP2/6-31G**

level of theory with PC-GAMESS [18,19]. The *trans-gauche* conformer was calculated to be less stable by $\Delta E = 5.4$ kJ mol $^{-1}$ and to have a somewhat larger total dipole moment, 1.25 D, than the value of 1.09 D found for the *trans-trans* conformer. However, in contrast to the *trans-trans* species, where the total dipole moment is along the twofold principal inertial *b* axis, as can be seen in Fig. 1, the dipole moment of the *trans-gauche* species is oriented in the inertial axis system in such a way that there are three non-zero, but relatively small dipole moment components. With the calculated values of the three components, $\mu_a = 0.409$ D, $\mu_b = 0.792$ D, and $\mu_c = 0.872$ D, *b*-type and *c*-type transitions would be expected to be dominant in the *trans-gauche* spectrum, as is indeed indicated in Fig. 2. Nonetheless, the spectrum of the *trans-gauche* conformer was expected to be rather complex and at an intensity level appreciably lower than that of the *trans-trans* conformer.

The rotational spectrum of the *trans-gauche* conformer was identified and assigned in two steps. In the first step, a search was made for *b*- and *c*-type *Q* branches at a spacing close to the value $2A - B - C = 22.6$ GHz predicted from calculated rotational constants. The *Q* branches are indicated in Fig. 8 for *b*-type transitions, where, instead of a classic FORTRAT diagram, we plotted the logarithm of *b*-type transition intensities for *R* and *Q* branches versus

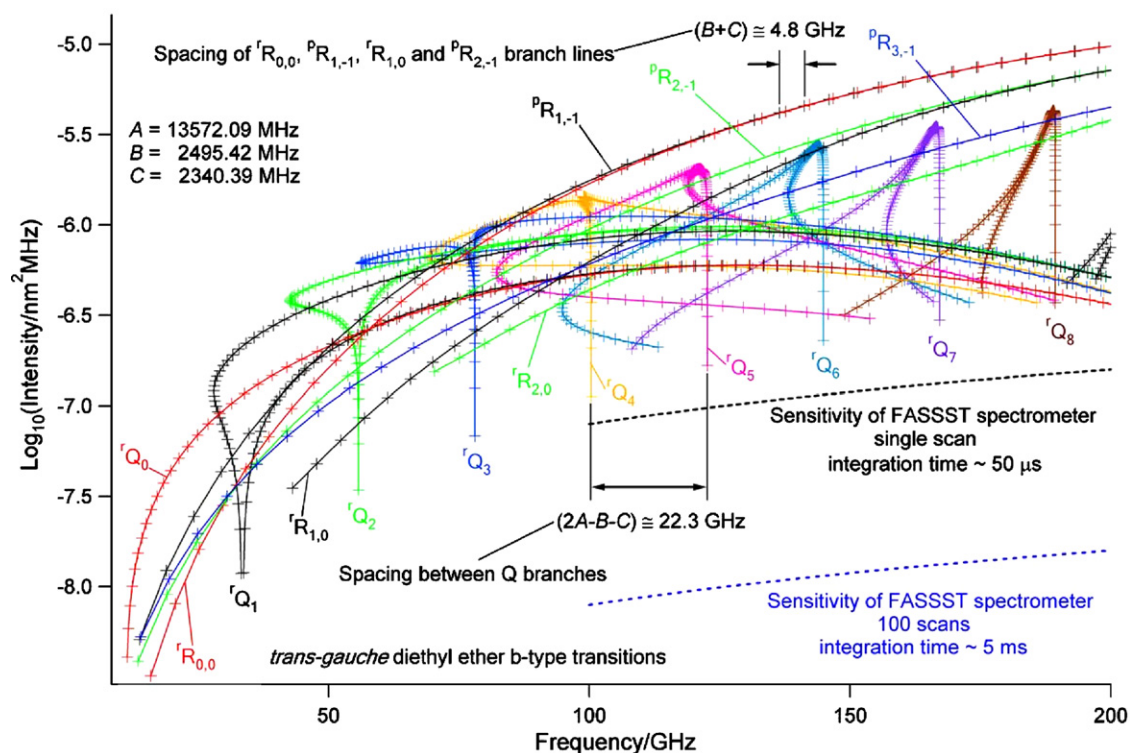


Fig. 8. Log_{10} (intensity) versus frequency plot for some *Q* and *R* branches of *trans-gauche* diethyl ether *b*-type transitions. The second subscript number of the *R* branches represents $(J'' - K_a'' - K_c'')$. The sensitivity of the FASSST spectrometer was calculated from the signal-to-noise ratio of SO_2 reference lines.

frequency. Fig. 8 also displays the sensitivity of the FASSST spectrometer for a single scan and 100 co-added scans. The spacing of 22.6 GHz was sufficiently different from the analogous spacing of 30.8 GHz found in the *trans-trans* conformer so that an unambiguous assignment was possible. An example of the superimposed *trans-gauche* *b*- and *c*-type ${}^rQ_{13}$ branches is shown in Fig. 9 with the experimental spectrum at the bottom trace and calculated frequency and intensity predictions at the top trace. This particular Q branch is accidentally close in frequency to the *b*-type rQ_9 branch of the *trans-trans* species so that initially it was considered to be a vibrational satellite of the latter. As it turned out, and is indicated in Fig. 9, the *trans-gauche* Q branches are characterized by considerably different K_a quantum numbers. Fig. 10 shows clearly the lack of obvious structure of the combined *b*- and *c*-type ${}^rQ_{15}$ -branch patterns at the higher value of $K_a=15$.

Once such a sequence of Q branches with a spacing close to 22 GHz was identified, and confirmed that the *trans-gauche* conformer is indeed observable, an attempt was made to assign transitions in the strongest *b*- and *c*-type R branches. Since the *trans-gauche* conformer is a near prolate rotor with an asymmetry parameter $\kappa=-0.972$, such transitions were expected to be those with the smallest values of the K_a quantum number. Some difficulty was encountered in assigning such transitions since they do not fall into obvious patterns, but are in the form of intermeshed combs, each

comb with spacing close to $B+C=4.8$ GHz, as shown in Fig. 8. Assignment of several such sequences was finally achieved and, in turn, also allowed the much weaker *a*-type transitions also to be identified. A further factor to consider in the analysis was that the strongest transitions often consisted of unresolved doublets or quartets involving both *b*- and *c*-type transitions. The transitions belonging to the R branches of the *trans-gauche* conformer, although readily measurable, give rise to patterns that are only discernible with some difficulty, since the spectrum is dominated by stronger lines of the *trans-trans* conformer, as can be seen from Figs. 2 and 9. Some such patterns are shown in detail in Fig. 11 for lines scattered in a dense region of the spectrum forming a K_a R -branch cluster belonging to the $J=32\leftarrow 31$ *a*-type rotational transition. Fig. 12 shows transitions due to all three non-zero dipole moment components of *trans-gauche* diethyl ether, including one of the *b*-type and *c*-type quartets mentioned above.

The Q branches and several *b*-type R -branches were in fact first identified in the PLL spectra and an initial set of spectroscopic constants was determined. Those constants were then used as input data for the computer aided assignment of asymmetric rotor spectra (CAAARS) program [20], whereupon a much larger number of lines measured with the FASSST system could rapidly be assigned.

The final data set acquired for *trans-gauche* diethyl ether is reported in Table S1 as electronically available supplementary material and consists of 1090 measured

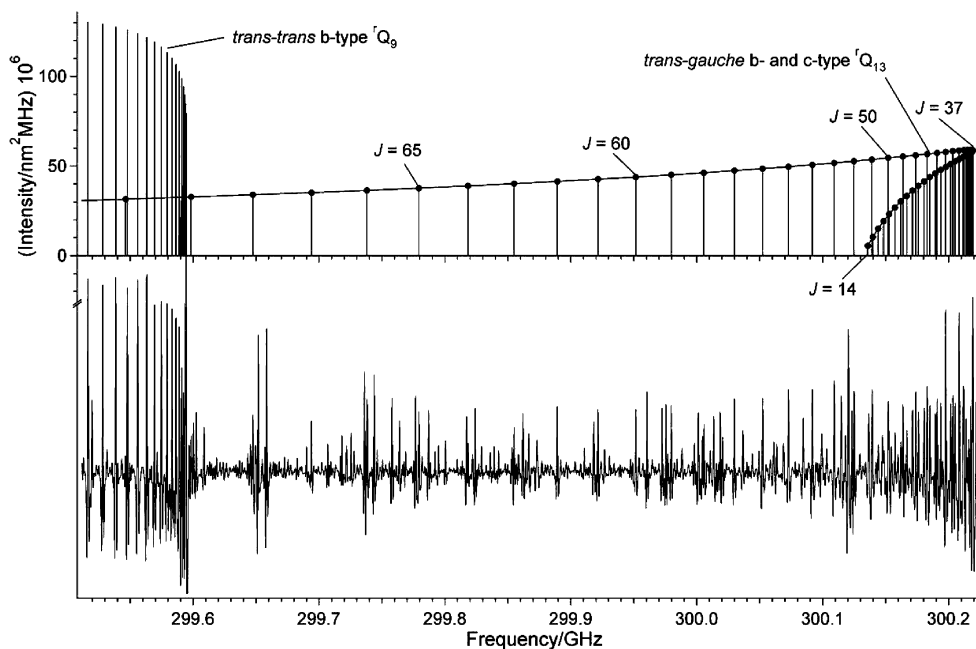


Fig. 9. An accidental near-coincidence between a Q branch of the *trans-gauche* conformer and a Q branch of the *trans-trans* conformer of diethyl ether. In the *trans-trans* Q branch each line consists of an unresolved asymmetry doublet, whereas in the *trans-gauche* Q branch each line represents an unresolved quartet arising from overlapped *b*- and *c*-type doublets. The two Q branches are characterized by considerably differing values of the K_a quantum number owing to rather different values of the A rotational constant in the two conformers. The upper plot shows the calculated line positions and intensities, while the lower trace displays part of the experimental spectrum.

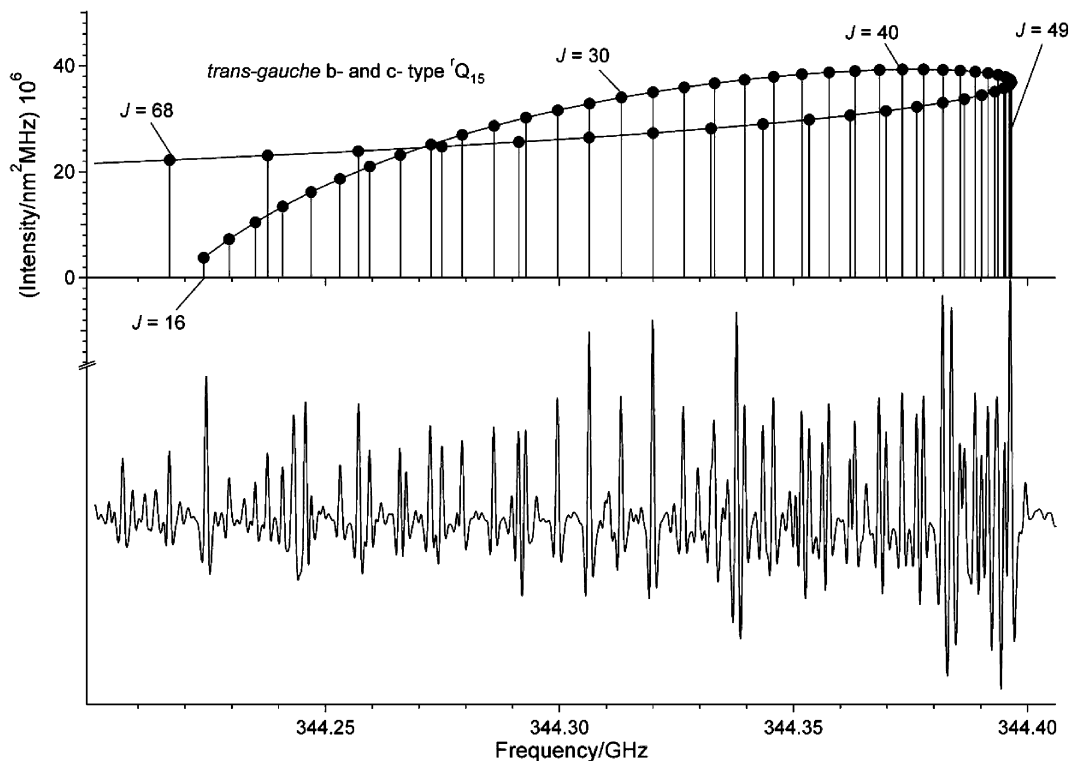


Fig. 10. *b*- and *c*-type Q -branch transitions of the *trans*-*gauche* conformer of diethyl ether in the submillimeter-wave region. The upper plot represents the calculated line positions and intensities, while the bottom trace shows the experimental spectrum.

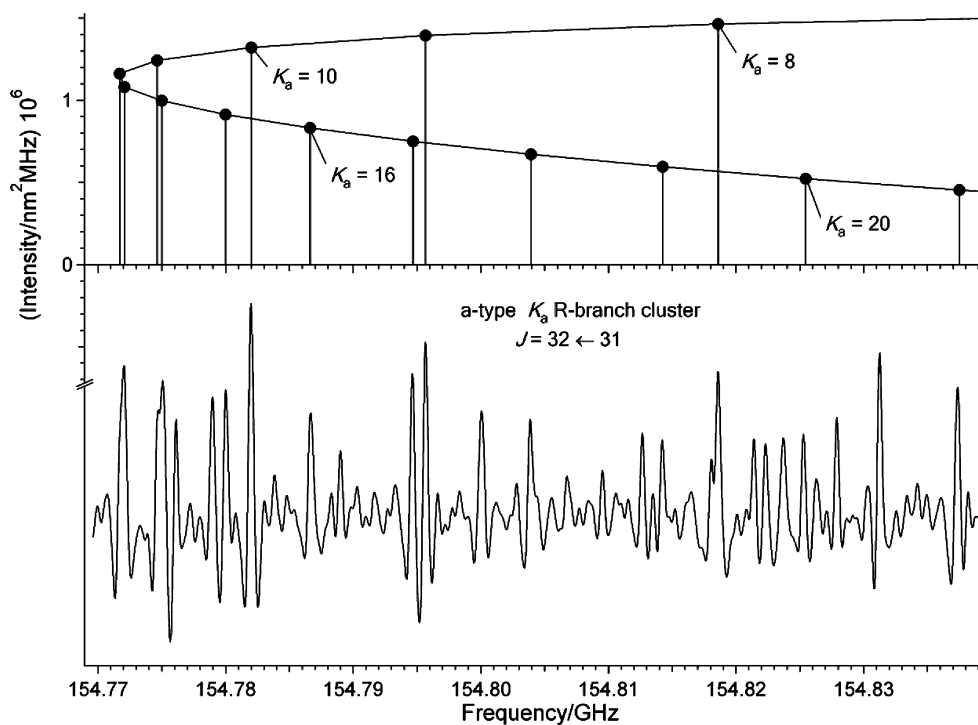


Fig. 11. *a*-type K_a R-branch cluster of *trans*-*gauche* diethyl ether. The top part of the figure indicates the calculated intensities for various values of K_a versus frequency. The bottom trace shows the experimental spectrum.

lines, many of which are multiplets. Unresolved multiplets with splittings >20 kHz were not included in the fit. Thus, 2130 individual transitions are entered in

Table S1. The PLL spectrometer provided 188 lines or 550 transitions, while the remaining 902 lines or 1580 transitions were obtained from the FASSST spectrum.

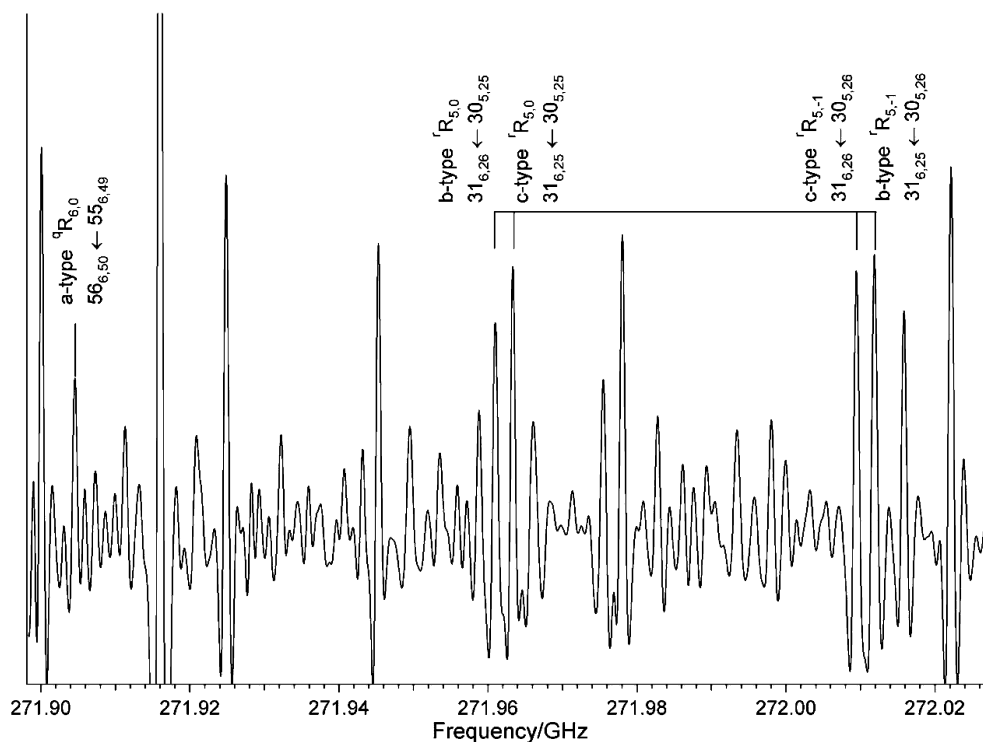


Fig. 12. Illustration of the different types of transitions observable for *trans-gauche* diethyl ether as a consequence of three non-zero dipole moment components. On the right-hand side of the graph we see a quartet of *b*- and *c*-type *R*-branch transitions between two pairs of rotational levels, close to a significantly weaker *a*-type *R*-branch transition. The strong line at 271.916 MHz is the $30_{5,25} \leftarrow 29_{4,26}$ transition of the *trans-trans* conformer and illustrates the relative weakness of the *trans-gauche* rotational spectrum.

Transition frequencies range from 108 to 366 GHz, with values of quantum number J'' in the range 4–77 for *R*-branch transitions and 11–79 for *Q*-branch transitions. The measured transition frequencies were fitted with constants in Watson's asymmetric rotor Hamiltonian [21], in the *A*-reduction and the *I'*-representation. The fitted constants are listed in Table 1, in which they are compared with values resulting from our *ab initio* calculation, as well as with corresponding values for the *trans-trans* conformer. The FASSST lines were weighted in the fit using an assumed frequency measurement error of 0.1 MHz, and an error of 0.05 MHz was used for the PLL lines. The overall deviation of fit 0.063 MHz, is seen to be acceptable although, in contrast to the *trans-trans* conformer, it was necessary to resort to constants up to the octic level of centrifugal distortion. In fact the constants in Table 1 represent the most economical set of constants, since a further small improvement in the standard deviation of the fit is still possible by adding more constants. The need for octic constants is not surprising since all quartic constants for the *trans-gauche* conformer are greater than those for the *trans-trans* conformer, and the important sextic constants H_{JK} , H_{KJ} , and H_K are all an order of magnitude greater. The appreciable increase in centrifugal distortion in the *trans-gauche* form is understandable since this conformer is confined within a

considerably shallower potential well. The barrier to the *trans-trans* form is calculated to be only 386 cm^{-1} , whereas in the reverse direction this is 837 cm^{-1} . The quartic centrifugal distortion constants are all seen to be in fair agreement with values calculated from the harmonic force field. The poorest correspondence, for Δ_{JK} and δ_K , is more likely to be the result of anharmonicity than of some spectroscopic interaction.

4. Population of *trans-gauche* conformer in the vapor of diethyl ether

4.1. Experimental value

The abundance of the *trans-gauche* (*tg*) conformer relative to the more abundant *trans-trans* (*tt*) species was evaluated from the rotational spectra by means of the formula

$$I_{tg}/I_{tt} = N_{tg}\alpha_{\max}^{tg}/(N_{tt}\alpha_{\max}^{tt}), \quad (1)$$

where I_{tg} and I_{tt} are the observed absorption intensities (absorptances) of *trans-gauche* and *trans-trans* lines in arbitrary units for both conformers, N_{tg} and N_{tt} are the corresponding amount concentrations of *trans-gauche* and *trans-trans* diethyl ether in the sample, and the quantities α_{\max}^{tg} and α_{\max}^{tt} are the calculated molar

Table 1
The experimental and the calculated spectroscopic constants for the two conformers of diethyl ether

	<i>trans–trans</i> Conformer, [1]		<i>trans–gauche</i> Conformer	
	Obs.	Calc. ^a	Obs.	Calc. ^a
<i>A</i> (MHz)	17596.15648(48)		13572.0904(11)	13710.0
<i>B</i> (MHz)	2244.225553(76)		2495.41982(17)	2492.0
<i>C</i> (MHz)	2101.793429(85)		2340.38842(15)	2334.4
Δ_J (kHz)	0.273924(24)	0.295	0.769546(56)	0.844
Δ_{JK} (kHz)	–3.64882(28)	–3.996	–6.32356(94)	–4.375
Δ_K (kHz)	85.9166(28)	89.93	106.416(10)	104.9
δ_J (kHz)	0.0329800(69)	0.0367	0.134543(24)	0.167
δ_K (kHz)	0.51277(66)	0.595	2.8683(39)	8.797
<i>H_J</i> (Hz)	0.0000749(23)		0.0000634(76)	
<i>H_{JK}</i> (Hz)	–0.002632(34)		0.1589(25)	
<i>H_{KJ}</i> (Hz)	–0.01776(80)		–1.5100(81)	
<i>H_K</i> (Hz)	0.1381(71)		–1.038(45)	
<i>h_J</i> (Hz)	0.00002671(76)		–0.0003068(39)	
<i>h_{JK}</i> (Hz)	0.0		–0.12143(95)	
<i>h_K</i> (Hz)	0.0		17.92(23)	
<i>L_{JJK}</i> (mHz)	0.0		–0.00633(45)	
<i>L_{JK}</i> (mHz)	0.0		–0.0067(11)	
<i>L_{KKJ}</i> (mHz)	0.0		–0.0795(80)	
<i>L_K</i> (mHz)	0.0		–1.0700(76)	
<i>l_{KJ}</i> (mHz)	0.0		–0.622(44)	
<i>N_{fit}</i> ^b	1010		1090	
σ_{fit} (MHz)	0.084		0.063	
σ_w ^c	0.926		0.736	

^a Calculated at the MP2/6-31G** level of theory. Quartic constants were evaluated from the harmonic force field scaled by 0.9 (0.95 in frequency), while rotational constants for *trans–gauche* diethyl ether were obtained by scaling the calculated geometry by the ratio between the experimental and the calculated geometry for *trans–trans* diethyl ether.

^b The number of distinct frequency lines in the fit.

^c Deviation of fit per unit weight.

naperian absorption coefficients, respectively. The assumption is made that the lines evaluated lie in the linear (optically thin) range of the Lambert–Beer law concerning the transmittances, and that the variation of BWO power can be neglected in a frequency interval of 25 MHz. Absorption coefficients were calculated using the ab initio dipole-moment components for the *trans–gauche* conformer— $\mu_a=0.409$ D, $\mu_b=0.792$ D, and $\mu_c=0.872$ D (calculated at the MP2/6-31G** level)—and the experimental value $\mu_b=1.0976(9)$ D [1] for the *trans–trans* conformer.

The calculated MP2/6-31G** dipole moment for the *trans–trans* conformer is 1.125 D and its proximity to the experimental value suggests that this level of calculation may also be adequate for the *trans–gauche* conformer. Relative intensity measurements were made, using the FASSST spectrum, on pairs of well-shaped, unperturbed lines belonging to the *R* branches of the *trans–trans* and *trans–gauche* species not farther apart than 25 MHz. Such pairs of lines range from 151 to 342 GHz in frequency; and low values of the K_a quantum number and a difference as small as possible in

the *J* quantum number were also a criteria in their selection. In the case of the *trans–trans* conformer the influence of spin statistics was neglected in the population evaluation, because for five pairs of equivalent hydrogen nuclei the product of the reduced nuclear statistical weight factor, $g_I \approx 1/2$, and of the symmetry number, $\sigma=2$, is very close to unity. Inclusion of spin statistics shows that the resulting difference in the *trans–gauche* abundance is approximately three times lower than the estimated rms error in the value of the abundance.

The resulting abundances of the *trans–gauche* conformer, $N_{ig}/(N_{ig} + N_{tt})$, are $29.8 \pm 0.8\%$ from an average of six comparisons between *b*-type *trans–gauche* transitions and those of the *trans–trans* lines, $31.7 \pm 1.0\%$ from four comparisons involving *c*-type transitions, and $30.4 \pm 1.6\%$ from eight comparisons using unresolved *b*- and *c*-type quartet lines. The lack of significant differences between various evaluations based on either *b*-type or *c*-type transitions provides additional evidence that at least the relative magnitudes of the calculated μ_b and μ_c dipole moment components for the *trans–gauche* form are fairly reliable. The preferred experimental value for the room

Table 2
Comparison of room temperature populations derived for the *trans-gauche* conformer of diethyl ether

ΔH (kJ mol ⁻¹)	$N_{ig}/(N_{ig} + N_{tt})$ (%)	Method	Reference
5.68	30.5(13)	Rotational spectrum	(This work)
	29.3	Ab initio	(This work)
	31(8)	Gas electron diffraction	[4]
4.81(44)	36(5) ^a	Raman vapor phase	[4]
5.74(40)	29(4) ^a	Liquid phase vibrational spectra	[5]
6.09(60)	26(5) ^a	Liquid phase vibrational spectra	[6]
6.49(40)	23(3) ^a	Liquid phase vibrational spectra	[6]

^a $N_{ig}/(N_{ig} + N_{tt})$ not reported and has been recalculated from the reported value for ΔH .

temperature population of the *trans-gauche* form is thus an average of all relative intensity comparisons, and is $30.5 \pm 1.3\%$. The value is in good agreement with the results of various previously determined population values for *trans-gauche* diethyl ether, summarized in Table 2.

4.2. Calculated value

The abundance of the *trans-gauche* conformer was calculated by starting from Eq. (4.48) of [22]

$$N_{ig}/N_{tt} = 2e^{-\Delta G^0/RT}, \quad (2)$$

where N_{ig} and N_{tt} are the isomeric amount concentrations of diethyl ether, and the factor 2 accounts for the existence of two equivalent minima at the *trans-gauche* conformation. The Gibbs free energy difference $\Delta G = 0$ for the equilibrium between the two isomers. Thus the enthalpy difference ΔH^0 and entropy difference ΔS^0 are expressed by

$$\Delta G^0 = \Delta H^0 - T\Delta S^0, \quad (3)$$

where $R = 8.31$ (J K⁻¹ mol⁻¹), $T = 298.15$ K. To a first approximation

$$\Delta H^0 = \Delta E + \Delta E_{zpe}, \quad (4)$$

where ΔE and the zero point energy difference ΔE_{zpe} were determined from ab initio calculations at the MP2/6-31G** level to be 5.40 kJ mol⁻¹ (452 cm⁻¹) and 0.278 kJ mol⁻¹ (23.2 cm⁻¹), respectively. The entropy difference in Eq. (3) was evaluated from $\Delta S^0 = R \ln(q_{ig}/q_{tt})$ where in the total partition functions q_{ig} and q_{tt} all components except the rotational ones were assumed to be equal. The resulting approximate expression $\Delta S^0 = R \ln(2.05)$ leads to $\Delta S^0 = 5.97 \times 10^{-3}$ kJ mol⁻¹ K⁻¹. This value is close to the value 6.49×10^{-3} kJ mol⁻¹ K⁻¹ from [4]. The resulting ab initio-based room temperature population of the *trans-gauche* conformer is 29.3% , in good agreement with the experimental value.

5. Discussion

The *trans-gauche* conformer has been unambiguously identified in the rotational spectrum of diethyl ether, as

confirmed by the correspondence between the observed and calculated rotational and quartic centrifugal distortion constants listed in Table 1. The experimental and calculated estimates of the room temperature population of this conformer made in this work are self-consistent and in agreement with previous determinations. Although the *trans-gauche* conformer constitutes an important fraction of the room temperature population of diethyl ether, it will be less populous with diminishing temperature. From Eqs. (2)–(4) the quantity $N_{ig}/(N_{ig} + N_{tt})$ is estimated to be 11.6% at 200 K and only 0.4% at 100 K. The ideal source in interstellar clouds for detection of the *trans-gauche* conformer of diethyl ether would then appear to be hot molecular cores, in the direction of which the tentative detection of the *trans-trans* conformer has already been claimed [23]. Since they are in proximity to young high-mass stars, such sources are much warmer than most parts of interstellar clouds, so that rotational spectra from excited torsional and even excited vibrational states can be found. For example, rotational lines from the excited *gauche* torsional state of ethyl alcohol have been detected in a hot core towards Orion KL [24] while rotational spectra from the excited in-plane bending state and the first excited torsional state of ethyl cyanide have been detected in the hot core Sgr B2(N-LMH) near the galactic center [25]. To aid astronomers in searching for the *trans-gauche* conformer, we will be glad to supply a table of predicted frequencies upon request.

It is intriguing that we were unable to observe the spectrum of the *trans-gauche* conformer in a supersonic expansion. In the preceding investigation of the *trans-trans* conformer [1] we used the centimeter-wave cavity Fourier-transform spectrometer to measure the dipole moment, and intended to also make Stark measurements on the *trans-gauche* form. The lack of a spectrum is attributable to the known effect occurring upon supersonic expansion, of condensation of less stable conformers to the most stable one if the barrier between them is relatively low [26]. This effect is more likely than relaxation via a dipole-allowed transition. The *trans-gauche* conformer was calculated to lie higher in energy by 5.40 kJ mol⁻¹ (452 cm⁻¹) than the *trans-trans* one, and to be separated from the global minimum by a relatively

moderate barrier of 386 cm^{-1} for rotation of the ethyl group around the C–O bond. In the similar case of ethyl formate [26], the barrier for conversion of the less stable conformer to the more stable one is also of comparable magnitude, estimated at 300 cm^{-1} . The less stable conformer is, however, higher in term value by only $(\Delta E/hc) = 40\text{ cm}^{-1}$. It could not be observed with Ar carrier gas, but was observable with He, which provides less efficient cooling upon expansion. In the present case, we were unable to observe the *trans-gauche* spectrum with either Ar or He, which is probably attributable to a considerably greater energy difference between the two lowest energy conformers in diethyl ether than is the case in ethyl formate.

Acknowledgement

The Columbus authors thank NASA and The Army Research Office for their support. The Warsaw authors acknowledge financial support from the Institute of Physics of the Polish Academy of Sciences.

Appendix A. Supplementary data

Supplementary data for this article are available on ScienceDirect (www.sciencedirect.com) and as part of the Ohio State University Molecular Spectroscopy Archives (http://msa.lib.ohio-state.edu/jmsa_hp.htm).

References

- [1] I. Medvedev, M. Winnewisser, F.C. De Lucia, E. Herbst, E. Yi, L.P. Leong, R.P.A. Bettens, E. Białkowska-Jaworska, O. Desyatnyk, L. Pszczółkowski, Z. Kisiel, *ApJ Suppl. Series* 148 (2003) 593–597.
- [2] S.B. Charnley, P. Ehrenfreund, Y.-J. Kuan, *Spectrochim. Acta A* (2001) 685–704.
- [3] P. Caselli, T.I. Hasegawa, E. Herbst, *ApJ* 408 (1993) 548–558.
- [4] N. Kuze, N. Kuroki, H. Takeuchi, T. Egawa, S. Konaka, *J. Mol. Struct.* 301 (1993) 81–94.
- [5] J.P. Perchard, J.C. Monier, P. Dizabo, *Spectrochim. Acta A* 27 (1971) 447–462.
- [6] I. Kanetsaka, R.G. Synder, H.L. Strauss, *J. Chem. Phys.* 84 (1986) 395–397.
- [7] D.T. Petkie, T.M. Goyette, R.P.A. Bettens, S.P. Belov, S. Albert, P. Helminger, F.C. De Lucia, *Rev. Sci. Instrum.* 68 (1997) 1675–1683.
- [8] S. Albert, D.T. Petkie, R.P.A. Bettens, S.P. Belov, F.C. De Lucia, *Anal. Chem.* 70 (1998) A719–A727.
- [9] S. Albert, F.C. De Lucia, *Chimica* 55 (2001) 29–34.
- [10] Labview <<http://www.labview.com/>> 11500 N Mopac Expwy, Austin, TX 78759-3504.
- [11] Igor Pro <<http://www.wavemetrics.com/>> WaveMetrics, Inc., P.O. Box 2088, Lake Oswego, OR 97035, USA.
- [12] H.M. Pickett, *J. Mol. Spectrosc.* 148 (1991) 377–377 Current program versions and JPL catalogue are available from: <<http://spec.jpl.nasa.gov/>>.
- [13] Z. Kisiel, O. Desyatnyk, L. Pszczółkowski, S.B. Charnley, P. Ehrenfreund, *J. Mol. Spectrosc.* 217 (2003) 115–122.
- [14] Z. Kisiel, E. Białkowska-Jaworska, L. Pszczółkowski, *J. Mol. Spectrosc.* 177 (1996) 240–250.
- [15] Z. Kisiel, L. Pszczółkowski, *J. Mol. Spectrosc.* 181 (1997) 48–55.
- [16] W.C. King, W. Gordy, *Phys. Rev.* 93 (1954) 407–412.
- [17] Z. Kisiel, PROSPE—Programs for ROtational SPEctroscopy. Available from: <<http://info.ifpan.edu.pl/~kisiel/prospe.htm>>.
- [18] M.W. Schmidt, K.K. Baldrige, J.A. Boatz, S.T. Elbert, M.S. Gordon, J.H. Jensen, S. Koseki, N. Matsunaga, K.A. Nguyen, S.J. Su, T.L. Windus, M. Dupuis, J.A. Montgomery, *J. Comput. Chem.* 14 (1993) 1347–1363.
- [19] A.A. Granovsky, PC-GAMESS program. Available from: <<http://classic.chem.msu.su/gran/gamess/index.html>>.
- [20] CAAARS program. Available from: <<http://www.physics.ohio-state.edu/~medvedev/caaars.htm>>.
- [21] J.K.G. Watson, in: J.R. Durig (Ed.), *Vibrational Spectra and Structure*, vol. 6, Elsevier, New York/Amsterdam, 1977, pp. 1–89.
- [22] W.J. Orville-Thomas (Ed.), *Internal Rotation in Molecules*, Wiley, London, 1974.
- [23] Y.-J. Kuan, Personal communication.
- [24] J.C. Pearson, K.V.L.N. Sastry, E. Herbst, F.C. De Lucia, *ApJ* 480 (1997) 420–431.
- [25] D.M. Mehringer, J.C. Pearson, J. Keene, T.G. Phillips, *ApJ*, in press.
- [26] T.D. Klots, R.S. Ruoff, H.S. Gutowsky, *J. Chem. Phys.* 90 (1989) 4216–4221.